Foundations and Trends® in Renewable Energy
Vol. 1, No. 1 (2016) 1–44

DOI: 10.1561/2700000006

now
the essence of knowledge

Spatial and Temporal Variability of Solar Energy

Richard Perez
University at Albany, SUNY, Albany, USA, rperez@albany.edu

Mathieu David
University of La Réunion, La Réunion, France,
mathieu.david@univ-reunion.fr

Thomas E. Hoff
Clean Power Research, Napa, California, USA,
tomhoff@cleanpower.com

Mohammad Jamaly
University of California, San Diego, California, USA,
smjamaly@ucsd.edu

Sergey Kivalov
University at Albany, SUNY, Albany, USA, skivalov@albany.edu

Jan Kleissl
University of California, San Diego, California, USA,
jkleissl@ucsd.edu

Philippe Lauret
University of La Réunion, La Réunion, France,
philippe.lauret@univ-reunion.fr

Marc Perez
MGH-Energy, Montpellier, France, mjp2167@columbia.edu

Contents

Abstract

This monograph summarizes and analyzes recent research by the authors and others to understand, characterize, and model solar resource variability. This research shows that understanding solar energy variability requires a definition of the temporal and spatial context for which variability is assessed; and describes a predictable, quantifiable variability-smoothing space–time continuum from a single point to thousands of kilometers and from seconds to days. Implications for solar penetration on the power grid and variability mitigation strategies are discussed.

R. Perez, M. David, T. E. Hoff, M. Jamaly, S. Kivalov, J. Kleissl, P. Lauret, and M. Perez. *Spatial and Temporal Variability of Solar Energy.* Foundations and Trends® in Renewable Energy, vol. 1, no. 1, pp. 1–44, 2016.
DOI: 10.1561/2700000006.

1

Introduction

Unlike conventional electrical power generation (e.g., fossil or nuclear), solar energy is intermittent. The output of a solar power plant is driven by weather and by the cycle of days and seasons. It varies from zero to full power outside the control of plant operators.

The intermittency, or better termed, variability, of the solar resource has two causes. One is precisely predictable and traceable to the apparent motion of the sun in the sky and the earth's distance from the sun. The other is much less predictable and traceable to the motion of clouds and weather systems.

In order to fully understand the issue and develop intelligent mitigation solutions, both solar geometry-induced variability and cloud-induced variability should be examined in an appropriate spatial and temporal context. Taking an intuitive example for the temporal context, a single location on a given partly cloudy day will experience a high degree of variability due to changes in solar geometry and the passing of clouds. However, solar energy integrated over several days at that same location will exhibit less variability and variability will become insignificant as the temporal integration increases to one year or more (Figure 1.1) — e.g., see Gueymard and Wilcox (2011). Likewise

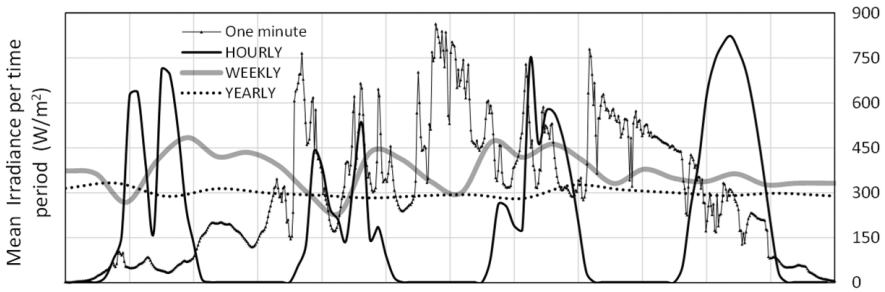

Figure 1.1: Comparing the variability of global irradiance time series in a North-American location, as a function of integration time. The figure includes 1 day's worth of one-minute data, 4 days' worth of hourly data, 26 weeks' worth of weekly data, and 16 years' worth of yearly-integrated data.

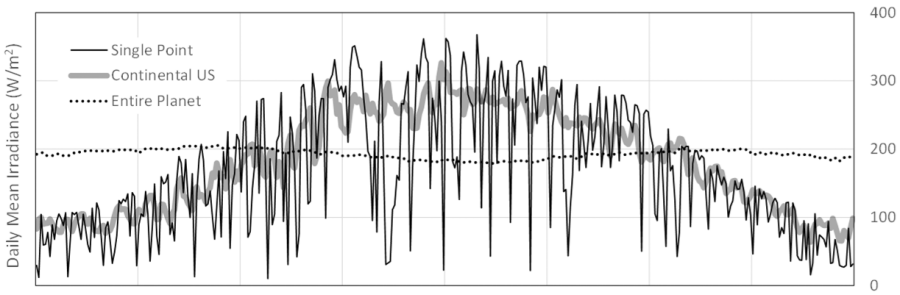

Figure 1.2: Comparing the variability of daily global irradiance time series for one year as a function of the considered footprint.

in the spatial realm, increasing the solar generation footprint from a single location to a resource dispersed over an entire region or a continent will reduce intermittency considerably. Increasing this footprint to the entire planet will eliminate it almost entirely (Figure 1.2).

The focus of this article is placed on understanding, characterizing, and modeling the interplay between intermittency and the considered spatial and temporal scales. Implications for the power grid and appropriate intermittency mitigation strategies are discussed.

2

Quantifying Intermittency

How is variability quantified? In this article we aim for a broad metric adaptable to a wide range of temporal and spatial scales and that describes: (1) the physical quantity that varies, (2) the variability time scale, and (2.1) the time span over which variability is assessed, noting that condition-specific characterizations of variability may be appropriate in particular circumstances such as, e.g., localized variability induced by cumulus fields [Tomson, 2009].

2.1 Physical quantity

The relevant quantity for energy producers and grid operators is the power output, p, of a power plant or an ensemble of power plants at a given point in time. As power output variability reflects the underlying variability of impinging irradiance, understanding and quantifying the variability of this irradiance amounts to quantifying and understanding the variability of p. The fundamental parameters by which irradiance can be quantified are global horizontal irradiance (GHI) and direct normal irradiance (DNI). The latter is most relevant

for concentrating technologies, while GHI variability is important for flat plate technologies.

Irradiance variability embeds both predictable solar-geometry, and cloud/weather effects. To focus on the latter, it is helpful to use a normalized quantity that removes solar geometry but conserves cloud-induced variability. The *clearness index, Kt* (ratio of GHI to extraterrestrial irradiance) or *the clear sky index, Kt^** (ratio of GHI to clear sky GHI) both meet this criterion, although many tend to prefer Kt^* because it more effectively removes solar geometry effects at lower solar elevations [e.g., see Perez et al., 1990] and has a more intuitive range.

2.2 Time scale

The above intuitive temporal example suggests that the time period or its inverse, the frequency, of the selected physical quantity's time series is an essential factor. Having defined the physical quantity, e.g., Kt^*, its variations $\Delta Kt^*_{\Delta t}$ over a given period Δt are often referred to as the ramp rates. The time interval can range from a few seconds to hours and more depending on the concern of the user.

2.3 Time span

A proper measure of variability should include ramp events over a statistically significant *time span*. This time span should be a large multiple of Δt.

2.4 Nominal variability metric

Nominal variability refers to the variability of the dimensionless clear sky index. The maximum or mean $\Delta Kt^*_{\Delta t}$ ramp rate over a given time span has been proposed as such a measure [e.g., Hoff and Perez, 2010]. However most authors prefer using the ramp rate's variance, or its square root, the ramp rate standard deviation, over a given time span

as the metric for variability. We retain this definition of *nominal variability*.

$$\text{Nominal variability} = \sigma(\Delta Kt^*_{\Delta t}) = \sqrt{\text{Var}[\Delta Kt^*_{\Delta t}]} \tag{2.1}$$

Historically, there have been other approaches to quantify variability. In earlier work, Skartveit and Olseth [1992] have used the standard deviation of Kt, σKt, rather than $\sigma\Delta Kt$ or $\sigma\Delta Kt^*$ as a measure of variability. However the latter should be considered a more appropriate metric because σKt can be driven by one single ramp event — consider for instance the case of perfectly clear conditions (i.e., no variability) followed by a one-time change to uniform, heavily overcast conditions without variability. In this case σKt would be the same as if conditions were highly variable and changing from clear to cloudy at every time period. On the other hand, $\sigma\Delta Kt^*$ would capture the difference between the two situations with a low value in the first case and a high value in the second.

2.5 Power output (absolute) variability

Equation (2.1) describes a nominal dimensionless metric. When dealing with power generation it is necessary to scale up the nominal metric and quantify power variability in absolute terms. This is expressed by Equation (2.2).

$$\text{Power variability} = \sigma(\Delta \mathbf{p}_{\Delta t}) = \sqrt{\text{Var}[\Delta p_{\Delta t}]} \tag{2.2}$$

3

Variability Mitigation — Spatial and Temporal Effects

When considering a fleet of multiple solar electric installations the power variability of N plants is given by [Hoff and Perez, 2012a, Perez and Fthenakis, 2012, Perez and Hoff, 2013]:

$$\text{Fleet power variability} = \sigma\left(\sum_{n=1}^{N} \Delta p^n_{\Delta t}\right) = \sqrt{\text{Var}\left[\sum_{n=1}^{N} \Delta p^n_{\Delta t}\right]} \tag{3.1}$$

where p^n represents the power output time series of the nth plant in the fleet.

In the special case where all the plants in the fleet are identical, exhibit the same variability $\sigma(\Delta p_{\Delta t})$, and their power output time series are *uncorrelated*, Equation (3.1) simplifies to:

$$\text{Fleet power variability} = \sqrt{N\,\text{Var}[\Delta p_{\Delta t}]} = \sqrt{N}\sigma(\Delta p_{\Delta t}) \tag{3.2}$$

In this special case, the *relative variability* — defined as the ratio of absolute variability to installed capacity — is given by:

$$\text{Fleet relative variability} = \frac{\sqrt{N}\sigma(\Delta p_{\Delta t})}{N P_{\text{installed}}} \tag{3.3}$$

where $P_{\text{installed}}$ is the installed capacity of each plant. Therefore the relative variability of a fleet of identical power plants with uncorrelated

power outputs, but experiencing the same level of individual variability, equals each individual plant's relative variability divided by the square root of the number of plants.

$$\text{Fleet relative variability} = (\text{Single plant relative variability})/\sqrt{N} \tag{3.4}$$

More generally, Equation (3.5) is applicable to the nominal variability of a fleet of N locations experiencing identical, but uncorrelated Kt^* time series.

$$\sigma_{\Delta t}^{\text{Fleet}} = \frac{\sigma_{\Delta t}^{1}}{\sqrt{N}} \tag{3.5}$$

where $\sigma_{\Delta t}^{\text{Fleet}}$ is the fleet's nominal variability and $\sigma_{\Delta t}^{1}$ is a single location's nominal variability.

This relative variability reduction underlies the well-known *spatial smoothing effect* noted by many authors — e.g., Marcos et al. [2012], Murata et al. [2009], Woyte et al. [2007], Wiemken et al. [2001], and Vignola [2001].

Nearby locations are highly correlated, experiencing the same ramp rates at the same time and varying in sync; in this case the fleet exhibits nearly the same relative variability as the individual systems. Distant locations' time series are uncorrelated; hence the fleet's relative variability is reduced by $\sqrt{N}$. Therefore the key factor to capture is correlation. A considerable amount of work has been devoted to this issue in recent years — e.g., Becker et al. [2014], Bing et al. [2012], Badosa et al. [2013], Frank et al. [2011], Halász and Malachi [2014], Hoff and Perez [2010], Huang et al. [2014], Jamaly et al. [2012], Kankiewicz et al. [2011], Kuszamaul et al. [2010], Lave et al. [2013], Lave and Kleissl [2013], Lorenz et al. [2011], Mazumdar et al. [2013], Norris and Hoff [2011], Perez et al. [2011,b, 2012], Rowlands et al. [2014], Sengupta [2011], Stein et al. [2011], Vindel and Polo [2014] — leading to the assertion that the correlation of $\Delta Kt^*_{\Delta t}$ time series between two locations is a predictable function of three factors:

- The distance, d, between the two locations,
- The time scale, Δt,

- The speed, V, of the variability-inducing clouds/weather systems.[1]

The central influence of time, speed, and distance had been identified by Hoff and Perez [2010] who postulated that a dimensionless *dispersion factor*, D, captures the variability relationship between a single point and a dispersed PV fleet. The dispersion factor is given in Equation (3.6) for a homogenous fleet of systems, where L represents the linear dimension of the fleet in the wind direction.

$$D = \frac{L}{V\Delta t} \tag{3.6}$$

They identified three possible fleet configurations (Figure 3.1):

1. A *crowded configuration* where the number of systems, N, exceeds the dispersion factor. In this case the relative variability of the fleet equals the single point's relative variability divided by D.

2. An *optimum configuration* where D equals N and where the fleet's variability equals the single point's variability divided by N.

3. A *dispersed configuration* where D is larger than N and where the fleet's variability asymptotically tends towards the single point's variability divided by $\sqrt{N}$ as D/N increases.

The dispersion factor model reflects the underlying correlation (or anti-correlation) existing between any two points within the fleet. Considering a single pair of stations experiencing the same nominal variability $\sigma^1_{\Delta t}$, Equation (3.5) may be generalized when the two locations are partially correlated, leading to:

$$\sigma^{\text{pair}}_{\Delta t} = \frac{\sqrt{\rho + 1}}{\sqrt{2}}\sigma^1_{\Delta t} \tag{3.7}$$

Where $\sigma^{\text{pair}}_{\Delta t}$ is the nominal variability of the pair and ρ is the correlation between each time series.

[1] This velocity is a priori defined as the vector in the direction of the two considered locations. However, as will be discussed latter, empirical evidence shows that a mean, local — directionless — velocity, can be an adequate input for assessing regional station pair correlations.

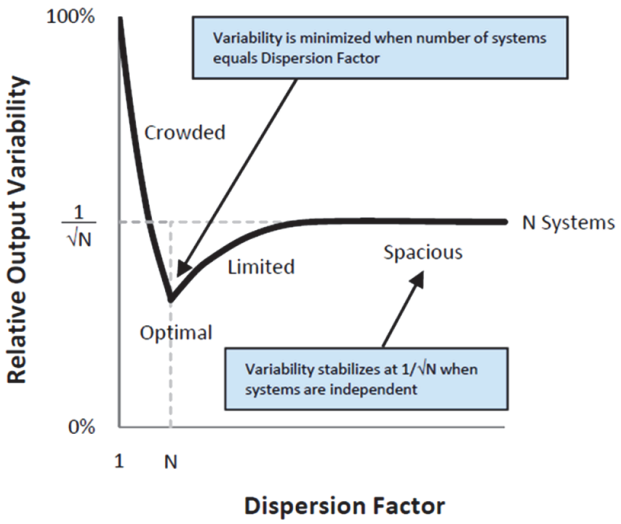

Figure 3.1: Relative output variability as a function of the dispersion factor for a fleet of N identical PV systems experiencing the same individual variability, [Hoff and Perez, 2010].

The dependence of ρ upon Δt, d, and V has been inferred from a growing base of empirical evidence.

Mills and Wiser [2010] analyzed 20-s data from the 32-station ARM network [Stokes and Schwartz, 1994]. They observed the exponential decay of station pair correlation as a function of station distance and noted that the rate of decay was a continuous function of the considered time scale. Hoff and Perez [2012a,b] used 10 km hourly satellite-derived irradiances over the continental United States. They observed a similar asymptotic decay with distance and a predictable dependence of this decay upon Δt for time intervals of 1, 2, and 3 h. They also noted that the rate of decrease of correlation with distance was different for different US regions and attributed these differences to prevailing regional cloud speeds. The analysis of high frequency data (seconds) from a 25-station modular network and confirmed that asymptotic decay with distance was a strong function of Δt depending on cloud speed that they had acquired independently from satellite-derived cloud motion

vectors [Perez and Hoff, 2013]. They proposed the following relationship linking distance, time interval, and cloud speed.

$$\rho = \frac{1}{1 + \frac{d}{(\Delta t)(V)}} \tag{3.8}$$

Perez et al. [2011] analyzed high-resolution, high-frequency, satellite-derived irradiances (1 km, 1 min) in climatically distinct regions of North America and Hawaii to investigate site-pair correlation decay as a function of distance (0–200 km) time scale (1 min to hourly) and mean monthly regional cloud speed (Figure 3.2) independently derived from satellite cloud motion vectors. They proposed an alternate formulation for ρ given in Equation (3.9):

$$\rho = e^{\frac{d \ln(0.2)}{1.5(\Delta t)(V)}} \tag{3.9}$$

Lave and Kleissl [2010] and Lave et al. [2011] analyzed high-resolution distributed irradiance measurements with a variety of statistical tools such as spectra, coherence spectra, wavelet, correlations, probability density functions, and spatial and temporal averaging with the objective of developing a model for simulating the power output of large power plants from single point measurements. The wavelet variability model (WVM) was then proposed in Lave et al. [2013] and it uses wavelet decomposition of the irradiance signal into different time scales (duration of shading from clouds or clouds systems), (Figure 3.3) that were proven to be associated with different amounts of variability reduction. The associated preliminary spatio-temporal correlation function dictates the amount of variability reduction and uses a parameter A that scales the correlation function and that had to be determined from a sensor network collecting high frequency irradiance data.

$$\rho = \exp(-\frac{d}{A\bar{t}}) \tag{3.10}$$

Through a virtual cloud model, Lave and Kleissl [2013] inferred that the parameter A in Equation (3.10) could be approximated to $1/2\ V$ for station pairs in the direction of the cloud speed.

Figure 3.4 illustrates and contrasts the formulations in Equations (3.8)–(3.10) for an example with a time scale of one minute and

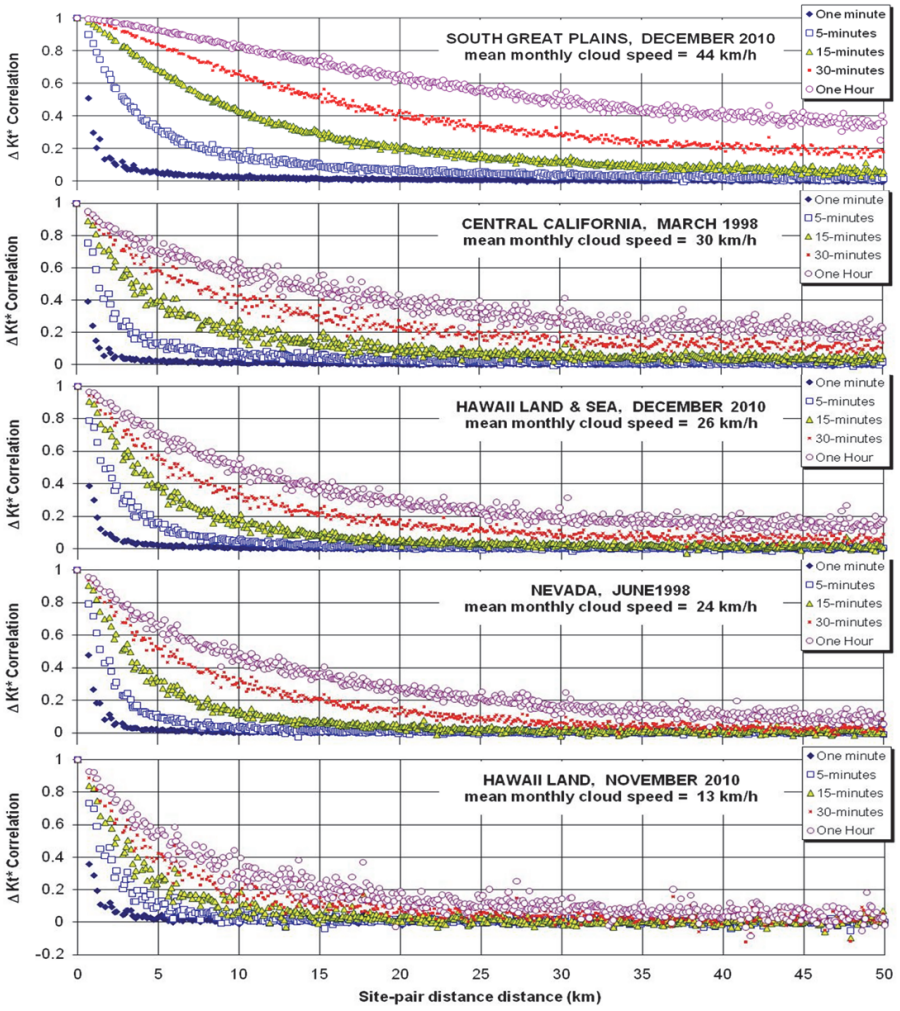

Figure 3.2: Site-pair correlation as a function of time period and distance for sample regions in North America and Hawaii. Mean monthly cloud speed was estimated from satellite-derived cloud motion vectors computed for each data point [Perez et al., 2011].

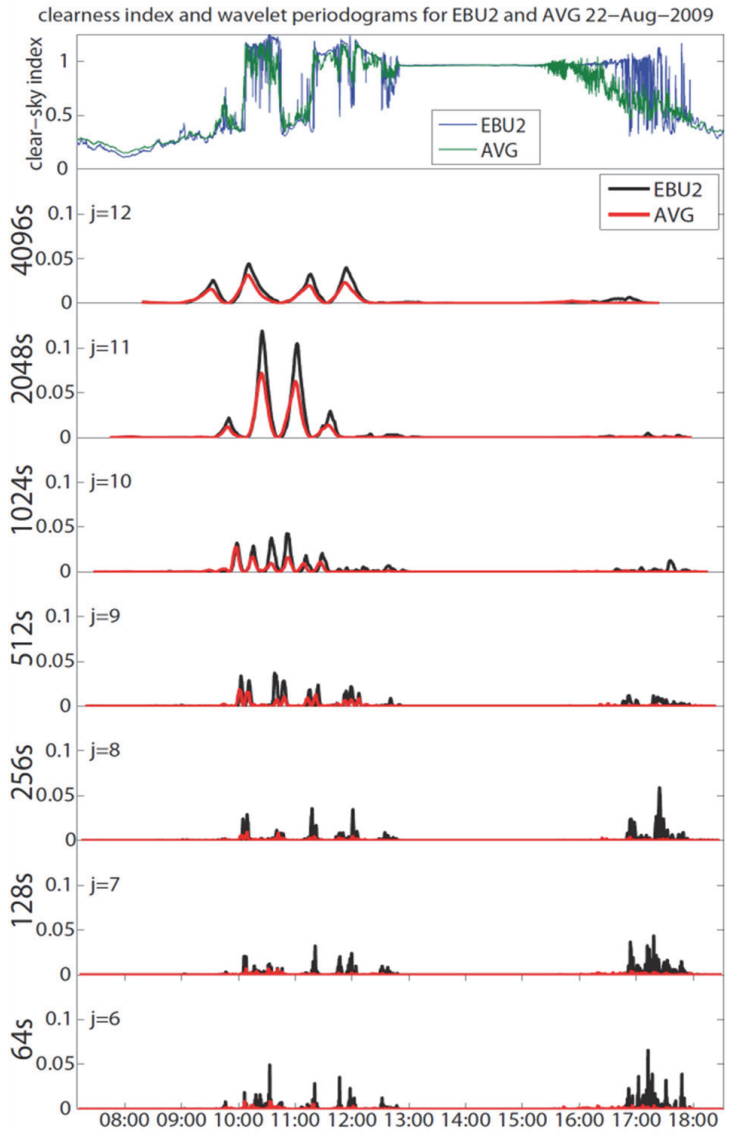

Figure 3.3: Clear-sky index (blue and green thin lines) and wavelet periodogram (black and red thick lines) of modes j = 6–11 for one site at UC San Diego (EBU2) and the average of six sites on August 22, 2009 (reproduced with permission from Lave et al., 2011).

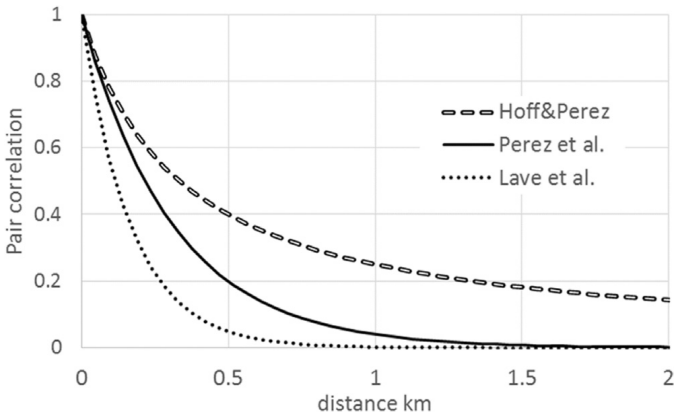

Figure 3.4: Comparing correlation decay with distance as formulated in Equations (3.8)–(3.10) for one-minute data and a cloud speed of 20 km/h.

a cloud speed of 20 km/h. Note that the difference between Equations (3.8) and (3.9) may be traceable to the fact that V represents a monthly prevailing cloud speed in the first case and a time-coincident cloud speed in the second, further noting that Equation (3.8) was derived empirically without consideration whether pairs where located along or across wind direction.

Formulations such as Equation (3.8) or (3.9) that define cloud speed in the direction of a station pair, do not explain the variability and correlation reduction with distance that is nevertheless observed when speed is zero — i.e., in cross wind directions — e.g., see Hinkelmann [2013], Lonij et al. [2013a,b]. As an attempt to describe correlation anisotropy with respect to cloud speed, Arias-Castro et al. [2013] applied a kinematic-stochastic model based upon given cloud cover fraction λ_n, cloud size r, stream-wise and cross-stream distance, cloud speed, and time difference. Through dimensional analysis, the correlation functions were expressed through just four independent variables: cloud cover fraction, the along-wind and cross-wind distance normalized by cloud diameter ($D_{\text{along}} D_{\text{cross}}$), and the distance of cloud motion within the ramp interval Δt relative to the cloud diameter

(D_{cloud}) resulting in Equation (3.11).

$$\rho = \frac{\begin{array}{r} 2e^{-\lambda_n}[2 - A_n(\sqrt{D_{\text{along}}^2 + D_{\text{cross}}^2})] \\ -e^{-\lambda_n}[2 - A_n(\sqrt{(D_{\text{along}} - D_{\text{cloud}})^2 + D_{\text{cross}}^2})] \\ -e^{-\lambda_n}[2 - A_n(\sqrt{(D_{\text{along}} + D_{\text{cloud}})^2 + D_{\text{cross}}^2})] \end{array}}{2[e^{-\lambda_n} - e^{-\lambda_n}[2 - A_n(D_{\text{cloud}})]]} \tag{3.11}$$

Further, the three key factors governing the correlation decay — time scale, cloud speed, and distance — are not entirely independent variables. This was noted by David et al. [2014] when they analyzed station pair correlations from an irradiance measurement network in the Island of La Réunion. Whereas exponential formulation in Equations (3.8) and (3.9) would imply that, for a given cloud speed, a linear relationship should exist between the distance at a given correlation level and time scale, with the slope depending on cloud speed [Perez et al., 2011], they observed that the time scale vs. distance slope tended to diminish as a distance increased (Figure 3.5). This may be explained by the observation that the underlying driver of variability (cloud speed) evolves as a function of the considered spatial and temporal scales. For the smallest scales, the drivers are cloud substructures. As the spatial scale increases, the drivers become entire cloud fields, and then entire weather systems, hence because the speed of these drivers is known to decrease with scale, the observed relationships are nonlinear.

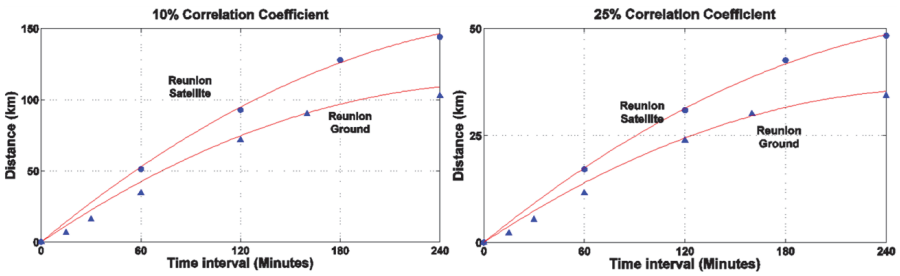

Figure 3.5: Mean distance to reach a 10% (a) and a 25% (b) correlation threshold as a function of the time interval of observations in La Reunion (ground and satellite) [David et al., 2014].

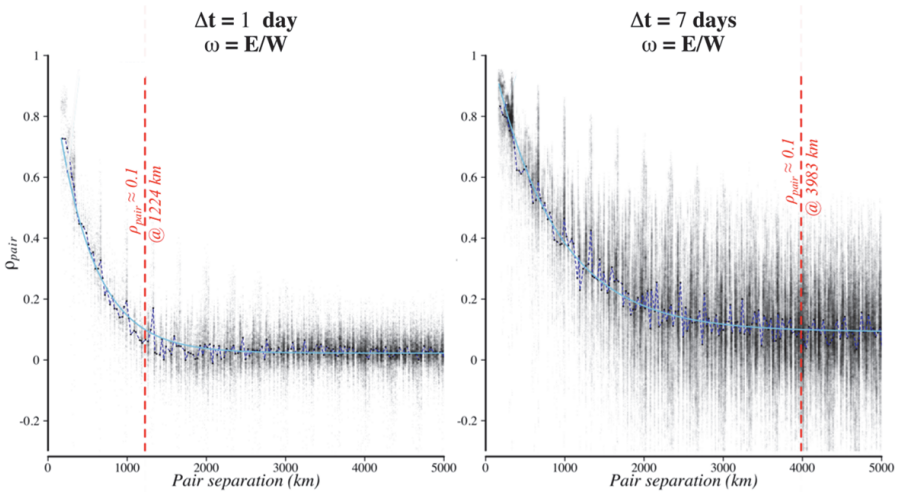

Figure 3.6: Site-pair correlation as a function distance for daily and weekly time periods. Station pairs are selected to have a predominantly east–west orientation [Perez and Fthenakis, 2015].

The cloud speed dependence upon time scale becomes fully apparent when considering very large spatio-temporal scales as in Perez and Fthenakis [2012], Perez et al. [2015] who analyzed millions of possible pair correlations from the NASA SSE data set [NASA SSE, 2012] for the entire planet. Figure 3.6 compares the observed exponential correlation decay for ΔT of 1 and 7 days, respectively. It is remarkable that these results are fully consistent with lower spatio-temporal scales such as shown in Figure 3.2, plausibly representing an expression of the underlying self-similar (fractal) nature of clouds and cloud systems at all scales [Lovejoy, 1982]. As for smaller scales, decorrelation distances are a function of prevailing cloud speed. Comparing east–west pairs and north–south pairs in Figure 3.7 indicates that decorrelation distances are considerably shorter for the latter — a manifestation of the fact that weather systems tend to move in east–west directions. Finally, as noted for La Réunion it is also apparent that the cloud system velocity underlying variability decreases with time scale. For instance, cloud system speeds inferred from Figure 3.7 using Equation (3.8) would

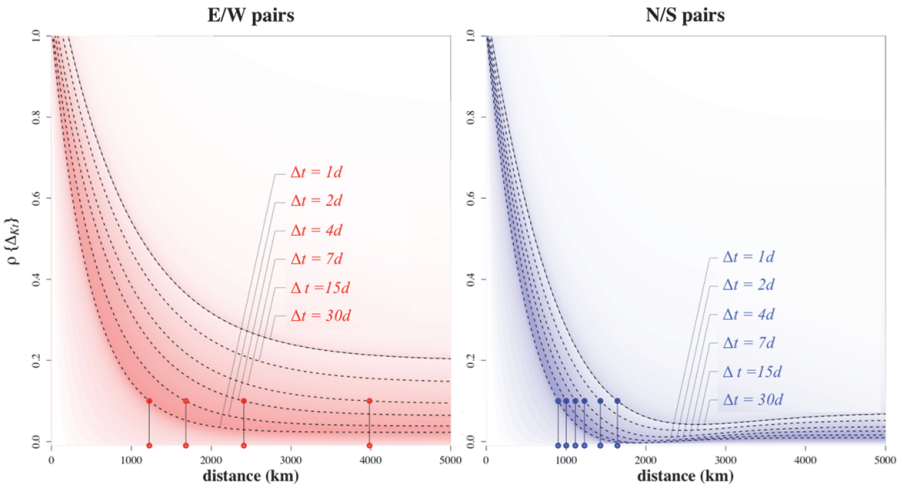

Figure 3.7: Impact of prevailing cloud speed on correlation decay for time periods ranging from 1 to 30 days — contrasting east–west pairs (prevailing direction of weather systems) and north–south pairs [Perez and Fthenakis, 2015].

indicate that the speed of the east–west weather system motion driver for daily ΔT is of the order of 20 km/h. For ΔT of 7 days the prevailing weather system's speed is of the order of 8 km/h.

4

Application Models and Tools

Understanding the fundamentals of solar resource variability's spatio-temporal characteristics has led to the development of tools and methodologies to address operational questions, in particular to address the question of how to predict the variability and output ramp-rates of spatially extended or distributed solar power plants from a limited number of input data, e.g., a single pyranometer.

4.1 Predicting variability of an extended source from a single or multiple measurement points

We discuss below, examples of direct application of the spatial/temporal variability correlations discussed earlier. In a following section, we also provide a detailed description of approaches based on kriging capable of providing spatially resolved variability from a limited number of sampling points.

An approach developed by Lave et al. [2013] applies the wavelet analysis to decompose the irradiance signal into different time scales (see Figure 3.3) to simulate a power plant's output given (1) a spatio-temporal correlation function (e.g., from Equation (3.10)),

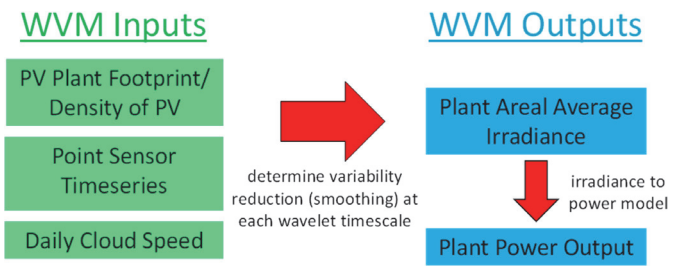

Figure 4.1: Wavelet variability model (WVM) for modeling reduction in PV power output variability through geographic smoothing [Lave et al., 2013].

(2) measurements from a single irradiance point sensor, (3) knowledge of the power plant footprint and PV density (Watts of installed capacity per m^2), (4) a time- and location-dependent scaling parameter (parameter A in Equation (3.10)). The Wavelet variability model (WVM, Figure 4.1) uses these inputs to estimate the variability ratio over the area of the plant. The simulated power plant may have any density of PV coverage: it may be distributed generation with low PV density (i.e., a neighborhood with rooftop PV), centrally located PV as in a utility-scale power plant with high PV density, or any combination thereof.

Another operational approach proposed by Hoff and Perez [2012a,b] is based upon expressing Equation (3.1) as the sum of the covariance of all possible plant pair combinations in a PV fleet.

$$\sigma_{\Delta t}^{\text{fleet}} = \sqrt{\text{Var}\left[\sum_{n=1}^{N} \Delta P_{\Delta t}^{n}\right]} = \sqrt{\sum_{i=1}^{N}\sum_{j=1}^{N} \text{COV}(\Delta P_{\Delta t}^{i}, \Delta P_{\Delta t}^{j})} \tag{4.1}$$

The covariance between any two plants equals the standard deviations of each of the locations times the correlation coefficient between the two locations (i.e., $\text{COV}(\Delta P_{\Delta t}^{i}, \Delta P_{\Delta t}^{j}) = \sigma_{\Delta t}^{i}\sigma_{\Delta t}^{j}\rho_{\Delta t}^{i,j}$). Therefore, the standard deviation of the changes in fleet output can be defined entirely by the standard deviation of the change in plant output at each location and the correlation between the locations (obtained from Equation (3.8)). This method can be applied by deriving nominal

variability from one, or a small subset of instrumented stations and assuming that sampled variability is representative of nearby locations.

Kato et al. [2011] proposed a comparable approach to determine fluctuation of high-penetration photovoltaic power generation systems dispersed over a large area known as the representative blocks method. PV is distributed over a number of subgroups each consisting of N blocks with a given installed capacity and a given variability. The size of each block is set such that block-to-block correlation is negligible and a form of Equation (3.3), accounting for different system sizes, may be applied to aggregate blocks and determined the variability of the ensemble.

4.2 Inferring spatial variability from gridded data sources

Recent years have seen the development of instruments and models capable of producing accurate irradiance data on extended spatial grids. Sky imagers can yield high spatial and temporal resolution data on footprints approaching 100 km^2 [e.g., Nguyen et al., 2016]. Satellite models [e.g., Perez et al., 2015] can produce gridded data for entire continents albeit at lower spatial and temporal resolution than sky imagers. With such massive input, and within their domain of applications, the problem of applying models to infer spatially extended variability does not pose itself since the extended variability information is inherent the gridded data.

However, the methodologies developed to understand variability have contributed to the enhancement of these instruments and models. The sky imager functionality has been greatly enhanced — Urquhart et al. [2014], to produce high frequency (seconds) locally gridded irradiance data (∼5 km radius) and cloud speed can be measured as input to variability models [Fung et al., 2014, Bosch and Kleissl, 2013, Bosch et al., 2013]. Satellite-to-irradiance models were also enhanced to produce high-resolution (1 km) data with a timescale approaching 1-minute [Perez et al., 2011]. In addition to producing the experimental data that led to a better understanding of variability, these new capabilities, in particular the satellite capability, have also led to a

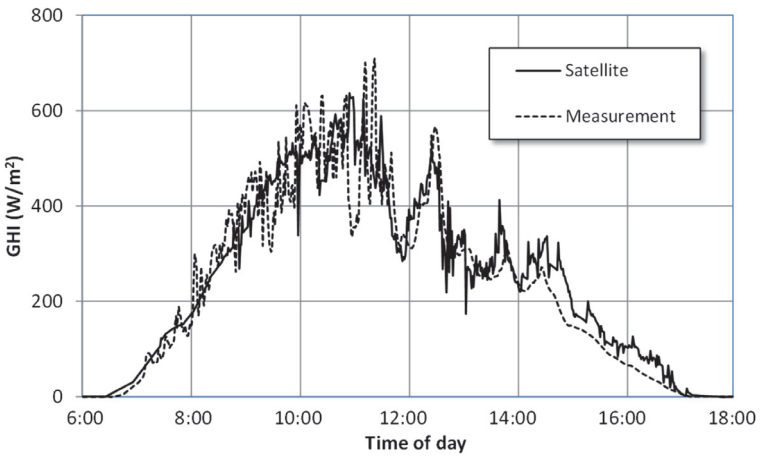

Figure 4.2: Comparing one-minute satellite-derived and measured global irradiance.

direct massive approach of PV fleet simulation to directly evaluate and manage variability issues for time scales in excess of a few minutes and spatial scales of a few kilometers, by directly simulating any dispersed PV fleets from satellite-derived irradiance time series [Clean Power Research, 2012]. An example of high-resolution, high-frequency satellite derived irradiance is shown in Figure 4.2.

In addition, combining the high-resolution satellite data capability with an understanding and parameterization of underlying variability and localized spatio-temporal correlations could open the door to improving short-term solar forecasts under high variability (partly cloudy) conditions [Zagouras et al., 2015].

5

Spatio-temporal Kriging — A Practical Approach to Infer Underlying Situational Space–time Variability

As noted in the first section of this document, the relationship characterizing point-to-point variability correlation is well documented from a wealth of empirical evidence — effects of time, space, and cloud/weather motion are well understood and parameterized, delineating a coherent continuum from ΔTs of seconds to several days and spatial scales ranging from meters to thousands of kilometers.

However, it is sometimes useful to describe time site-specific situations (decorrelation trends, directional effects traceable to localized conditions). Kriging offers the means of doing so from a limited number of measured data points. As mentioned earlier, this method would only be useful for spatial and temporal scale below what can be achieved by satellites today — where a deterministic use of gridded data would be a straightforward way to proceed — noting that both spatial and temporal resolution of future satellites will be improving.

Ground measurements of solar irradiance are sparse and continuous high quality measurements require more effort in maintenance and data quality control than common meteorological state variables [Vignola et al., 2013]. On the other hand, there exists a need for fully resolved (time steps on the order of seconds and grid resolution on the order

of 10 m) spatio-temporal irradiance data in applications such as solar power output in distribution feeder power flow simulations [Nguyen et al., 2016] and nearest-term forecasting of power output from large power plants [Lipperheide et al., 2015]. Linear or other common interpolation techniques may be appropriate to estimate the average annual solar resource at unobserved locations, but are inappropriate to create such temporally resolved irradiance data at unobserved locations. Linear interpolation, for example, reduces the solar radiation variance at unobserved locations and does not preserve spatial correlation properties. Satellite data, on the other hand, provides spatially continuous data that mitigates the need for spatial interpolation. Nevertheless for the aforementioned applications its coarse temporal resolution at 15–30 min and large pixel size (1 km or more) motivates a need for temporal downscaling or spatial interpolation. However, future satellites such as GOES-R may "eat away" at the operating space of spatio-temporal interpolation methods as the envisioned satellite spatial resolution of 500 m and temporal resolution of 5 min will promote the application of "raw" irradiance data in the aforementioned applications.

Kriging is a technique that can be applied to high fidelity solar resource modeling at unobserved locations. Kriging was first developed as a geostatistical interpolation method for spatial statistics [Krige, 1951]. Kriging is essentially a stochastic interpolation method where, in contrast to deterministic interpolation techniques that use only mathematical functions, both analytical and statistical methods are applied to predict unknown values based on correlation among data points. Kriging preserves the mean and correlation properties and also estimates the error of the process (kriging variance) which provides a basis for stochastic simulation [Burrough and McDonnell, 1998]. In many different fields of study kriging methods have been shown to be the best linear unbiased prediction method superior to deterministic interpolations procedures [Tabios and Salas, 1985, Buytaert et al., 2006, Jarvis and Stuart, 2001, Chuanyan et al., 2005].

Kriging formulation can be easily generalized to handle applications where the interpolant changes in time and space as is the case for solar resource modeling. Various forms of such spatio-temporal kriging are

used in solar engineering [Rehman and Ghori, 2000, Alsamamra et al., 2009, Bland and Clayton, 1994, Chen et al., 1994, McKenney et al., 2008, Merino et al., 2001, Moreno et al., 2011]: simple kriging assumes that the mean of the process across space and time is known. Otherwise, ordinary kriging (assuming unknown but constant mean) and universal kriging (assuming the unknown mean is a known function of co-variates, e.g., latitude, longitude) can be used. More advanced kriging methods are also applied for solar radiation forecasting [Alsamamra et al., 2009, Hengl, 2007, Antonanzas et al., 2015].

One of the important features about the kriging method is its ability to model as well as forecast solar radiation off-site. In other words, spatial interpolation or temporal downscaling can be performed. Therefore, the method can be applied to both ground-measured as well as satellite-derived solar irradiance data. For spatial interpolation, it is mostly advantageous for ground data, where available data are typically unstructured and sparse. However, when it comes to temporal downscaling or forecasting, the method would be promising for both satellite and ground data sets or their combination (as in the so-called co-kriging method, Dagostino and Zelenka, 1992, Journée and Bertrand, 2010). Gutierrez-Corea et al. [2001] concluded that when the simulation domain has adequate ground-station density, merging ground-measured and satellite-derived GHI data will improve the accuracy. On the contrary, when station density is low, the best method is estimating GHI directly from satellite images.

The main input to space–time kriging are space–time covariance functions. A parametric covariance function must be chosen (and parameters are calculated empirically, Dale et al., 2010, Dale and Zimmerman, 1989) based on some simplifications and assumptions including stationarity, separability, and isotropy. In a temporal (or spatial) stationary process, the mean and other statistical properties of solar radiation is constant over time (or space) and the covariance function is a function of time lags (or distance between locations) only; spatio-temporal stationarity of solar radiation is achieved if the process is stationary both spatially and temporally. If the covariance function is separable, spatial solar radiation variation is independent of

its temporal variation. Gneiting [2002], Gneiting et al. [2007] demonstrated special requirements for covariance functions and showed that they cannot be considered separable. In isotropic covariance functions, the covariance in solar radiation does not depend on direction. This assumption has been shown to be incorrect as the covariance along the direction of cloud motion is different than perpendicular to it [Hinkelmann, 2013, Perez et al., 2012, Lave and Kleissl, 2013, Arias-Castro et al., 2013]. Figures 5.1 and 5.2 demonstrate two different methods (spatial correlation and spatial cross-correlation), which show that this anisotropy is related to the cloud motion (or weather systems at large scales as discussed earlier.)

The semivariogram, another important function in the kriging method, is a function describing the degree of spatio-temporal dependence of solar radiation. Semivariogram is defined as the variance of the difference between solar radiation at two given points in space–time coordinates. For an (intrinsically) stationary process, the semivariogram is linearly related to the (parametric) covariance function. The most common covariance (and semivariogram) functions are in the form

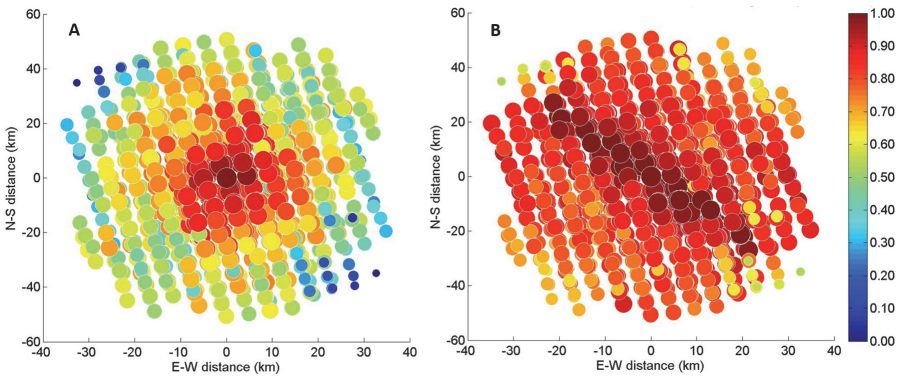

Figure 5.1: (a) Spatial correlation pattern of 1 min averaged kt of data from the Sacramento Municipal Utility District (SMUD) on January 24, 2012. (b) Spatial correlation between station pairs with the relative time-shift between stations adjusted to maximize cross-correlation. Correlation are visualized by the color scale as well as the size of the circle. Correlations are significantly increased for stations that are separated by a vector that is aligned with the cloud motion vector (here from 315°).

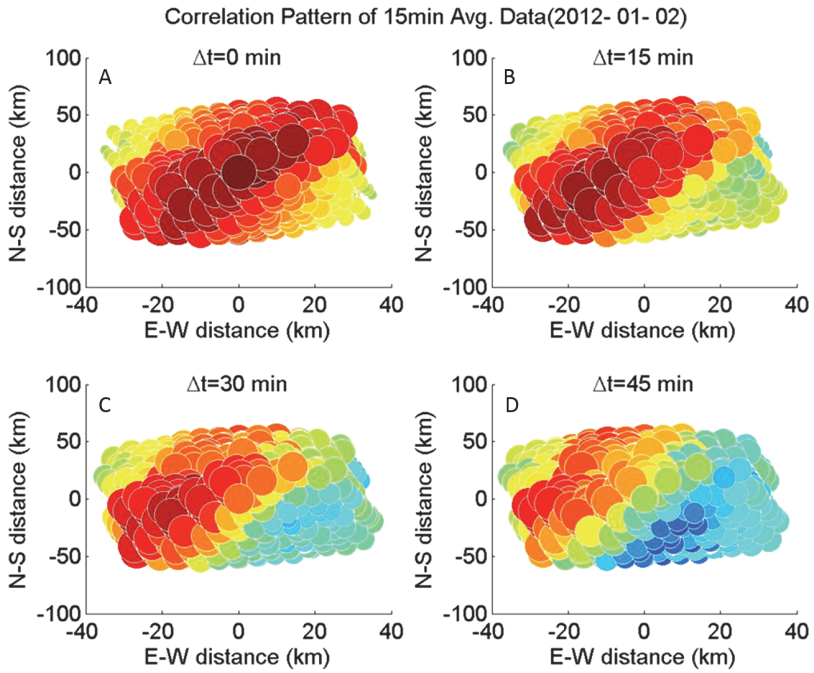

Figure 5.2: Correlation patterns of 15 min averaged kt of SMUD grid data for delays of (a) 0 min, (b) 15 min, (c) 30 min, and (d) 45 min. The blue (red) symbols represent positive (negative) correlation. The outer diameter corresponds to the size of the correlation.

of powered exponential, Whittle-Matern, and Cauchy functions. For example, Gneiting [2002] developed a general stationary nonseparable covariance function consisting of the powered exponential and Cauchy functions. Gneiting et al. [2007] also introduced stationary covariance functions that are not fully isotropic. They considered a physically motivated directional dependence of the covariance: the anisotropy is according to velocity vector of the flow, the covariance is a function of $(d - Vt)$ where d, V, and t represents the space, time, and velocity vectors, respectively. The motion vector for the Lagrangian reference frame can be obtained from the time delay of the maximum cross-correlations between all sites. This "Lagrangian" covariance function was shown to improve Irish wind forecasting [Gneiting et al., 2007].

Besides choosing an appropriate covariance function, stationarity and isotropy are required for accurate Kriging models. Temporal stationarity (and isotropy) is usually achieved by detrending solar irradiance time series usually through the clear sky index or clearness index [Inman et al., 2013]. Spatial stationarity is usually valid for small domains while spatial isotropy has to be established in a more sophisticated way according to cloud motion vector. The Lagrangian covariance function is applied in many studies to account for anisotropy occurred by cloud motion. Yang et al. [2013, 2014a], on the other hand, achieved spatial stationarity and isotropy through deformations of the geographical space based on the two-step method developed by Sampson and Guttorp [1992].

In general, the application of Lagrangian covariance functions is sensitive to accurate estimation of the cloud motion vector which is an emerging research area [Bosch and Kleissl, 2013, Bosch et al., 2013, Fung et al., 2014]. If a constant velocity vector (e.g., the average of the velocity field over the 8 hour period as in Inoue et al. — Inoue et al., 2012, Shinozaki et al., 2014) is assumed, temporal changes in cloud speed and/or direction degrade the accuracy of Kriging. As an alternative, the velocity field can be calculated at each time step using the cross-correlation method [Hamill and Nehrkorn, 1993].

To distinguish between along-wind and cross-wind correlations in solar radiation, Lonij et al. [2013b] considered a space–time covariance function as a product of a Lagrangian covariance function (in form of an exponential function) and a purely temporal one (in form of a powered exponential function). Inoue et al. [2012] considered a very similar covariance function. However, they considered a more complex Lagrangian term in the form of the covariance function proposed by Schlather [2010]. Applying the Lagrangian covariance function improves the Kriging method if a distinct cloud motion pattern exists. Therefore, considering a Lagrangian covariance function (where space is always combined with time through the cloud motion vector) along with a purely temporal one (without purely spatial term) may lead to results worse than the cases in which purely spatial covariance functions are applied as reported by Inoue et al. [2012]. So, as proposed

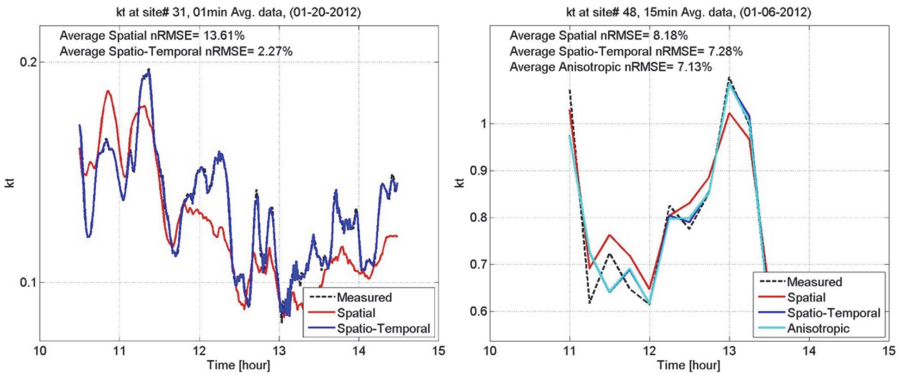

Figure 5.3: Sample of application of purely spatial and spatio-temporal ordinary kriging for 1 min (a) and 15 min (b) averaged data to model kt at an unobserved location. Anisotropic spatio-temporal Kriging (adding the Lagrangian covariance function similar to the one applied by Lonij et al. to the isotropic Gneiting covariance function as a convex combination) is also added on (b).

by Gneiting et al. [2007], using an isotropic nonseparable space–time covariance function along with such an appropriate Lagrangian one, as convex combinations, is a promising idea. Figure 5.3 compares spatial (using a powered exponential covariance functions) and spatio-temporal Kriging (using isotropic nonseparable Gneiting covariance function) for 1 min and 5 min averaged kt data.

Although applying an appropriate covariance function and ensuring stationarity and isotropy are key factors in successful applications of Kriging, reducing the size of the computations (and improving the results) by quantifying spatial and temporal decorrelation distances are the main practical challenges in applying the Kriging method for solar forecasting or interpolation. It has been widely demonstrated that the correlation decreases in distance and at some point irradiance time series at two sites will be uncorrelated [Perez et al., 2012, Lave and Kleissl, 2013, Arias-Castro et al., 2013, Lonij et al., 2013a, Perez and Fthenakis, 2015, Boudewijn and van Sark, 2013, 2014]. This distance is called spatial decorrelation distance (or effectiveness range or correlation length). A similar phenomenon is expected to occur in time (temporal decorrelation). Understanding spatial and temporal decorrelation

is very important which helps to reduce the computational cost since for a specific point and time only data within the spatial and temporal correlated zone are needed in the Kriging model. This is critical when the size of the problem (number of sites and/or time steps) is relatively large. For example, Yang et al. [2014a] applied parameter shrinkage, which applies spatial decorrelation (threshold distance) estimated using correlations from all directions and showed that it improves forecasting. The decorrelation also specifies a limit for interpolation and downscaling.

Unfortunately research on temporal decorrelation in solar energy literature is lacking. Yang et al. [2014a] presented circumstantial evidence on temporal decorrelation, hypothesizing that the temporal decorrelation can be quantified through the standard deviation of time lag distribution at the threshold distance. It should be noted that, mathematically, the temporal component in the spatio-temporal process is nothing but an additional dimension. Therefore, an inverse problem can be hypothesized to quantify the temporal decorrelation; i.e., at each given time lag, all the sites pairs whose maximum cross-correlation occurred at the given time lag are specified and the distance between these sites are calculated. The temporal decorrelation can be estimated by analyzing the standard deviation of the distance between the sites pairs against the time lags. Another promising method is to estimate spatial and temporal decorrelation analytically using the applied parametric covariance function. Moreover, if a Lagrangian covariance function exists in the parametric covariance function, the cloud motion effect can be evaluated by estimating along-wind decorrelation and decorrelation in other directions (including the cross-wind direction).

6

Implications for Power Grid Management

Observations and models describe a space–time continuum underlying the smoothing effect of solar resource variability: shortest-term variability matters for the smallest spatial scales while the minimum relevant time scale gradually increases with the size of the considered footprint. This is illustrated in Figure 6.1 where the absolute power variability of a nominal 1 kW PV power plant (from Equation (2.2)) is plotted as a function of the resource's footprint from a single point up to 200 × 200 km. This particular example is set in a tropical location. However, trends observed in different climates are quite comparable [Perez et al., 2013].

The solar generation footprint and time scale should therefore be the primary concerns of grid operators as they pose different load management challenges and imply different solutions: for single distribution systems and large centralized plants, one-minute fluctuations are relevant as they may create voltage control issues. For grid balancing areas including both fleets of large and small distributed systems, variability effects below 30 min should be of no concern, while hourly and above time scales remain relevant.

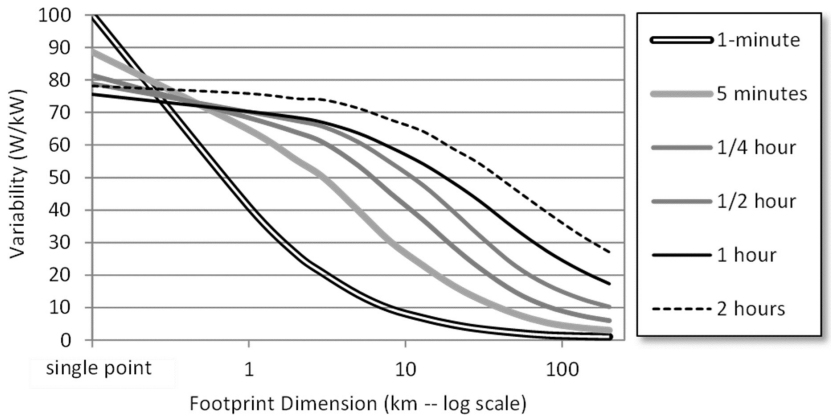

Figure 6.1: Nominal variability of a 1 kW power plant as a function of its footprint, Perez and Hoff [2013], Perez et al. [2013].

Likewise variability mitigation solutions should reflect the solar resource time–space context.

- Up to a few tens of meters — small and medium PV installations — ramp rates of the order of seconds are relevant — in particular over-irradiance issues, where ramps can exceed power ratings by up to 50% [Ole-Morten et al., 2014, Yordanov et al., 2013] and can create voltage control issues at interconnection points. These are generally passively mitigated by the installations' hardware that curtails excess spikes. For very large systems, buffering via capacitors may be warranted.

- From hundreds of meters to a few kilometers — distribution feeders and large PV plants — minute ramps are relevant, with impact on distribution system voltage, or transmission system voltage for large centralized power plants. In the latter case, active output buffering via capacitor or battery storage could be considered — some utilities impose maximum allowable one-minute ramp rate requirements [PREPA — Puerto Rico Energy Authority, 2013]. However, these should only be warranted for very large plants or very dense PV fleets where solar production

is of the order of the base demand energy flow on the local power grid. For most distributed systems, as long as penetration remains reasonable, experience shows that the ramping noise induced by PV systems on distribution grids is less than the background demand-side ramp noise that utilities have been accustomed to handle for a long time [Holger et al., 2014b,a]. For very large dispersed penetration — exceeding local demand — grid management would be similar to a centralized plant case and would require buffering.

- From 5 to 20 km — substations, cities — 1 minute variability vanishes while 10 minute and longer ramps remain. Depending on penetration, local regulation via storage may be needed.

- For ∼50 km — large cities and dense transmission networks — 15–30 min fluctuations and above are still a concern. Solutions include contingency stand-by generation, storage or load management in order to react to ramps and insure balance between supply and demand — note that these solutions need not be collocated with PV installations.

- For hundreds of kilometers — regional transmission organization's balancing areas — fluctuations of less than one hour should not be of concern. Variability mitigation at these scales can be effectively handled by an optimized basket of active generation, storage, load management, PV output curtailment, and increased interconnection bandwidth [Perez, 2015].

For all temporal and spatial scales where active variability mitigation would be needed, it has been shown that solar forecasting could substantially reduce mitigation measures and operational cost [Perez et al., 2013]. For small centralized scales, minutes-ahead forecasts could be obtained from sky imaging sensors [Yang et al., 2014b], while for a few kilometers and more, satellite-derived (1–2 h ahead) and numerical weather prediction forecasts (5+ hours ahead) would be warranted [Perez et al., 2014].

7

Conclusions

The most important observation reported in this article and assembled from a large body of work from recent years is the remarkable continuity and self-similarity of the relationships linking spatial footprint and temporal variability across a very large range of spatial and temporal scales, from seconds to days and from meters to thousands of kilometers. The long observed smoothing effect implying that variability is mitigated over space can be appropriately quantified from the knowledge of (1) the temporal scale, (2) the spatial scale, and (3) the motion of clouds or cloud systems — noting the latter is a second-order effect.

This observation implies that a proper understanding of how solar energy's resource variability impacts energy systems requires a definition of either the temporal or the spatial context for which variability is assessed. The shortest relevant timescale for which variability should be assessed is a direct function of the considered solar generation footprint, and, to a lesser extent, the speed of the clouds/weather systems inducing variability. For instance, when developing strategies to mitigate the impact of solar variability on electric power grids, defining this context is critical: indeed, whether one-minute ramps would be relevant for large centralized plants injecting solar kWh on the grid, focusing on

these short-term ramps would be useless and unproductive for fleets of small and medium power plants distributed over a utility service area, where mitigation occurs naturally.

The understanding of underlying variability structures has led to development of methodologies and models capable of extrapolating the resulting variability on arbitrarily defined spatial footprints (e.g., an ensemble of power plants) from a small sample of point measurements. These new models fill a gap in temporal and spatial scales, improving the temporal/spatial resolution of massive gridded solar data resources where all relevant variability information would be included in the data themselves without the need for models. The boundary between the two approaches is of the order of a few minutes on the temporal scale and a few kilometers on the spatial scale, noting that future satellite-derived data will push this operational boundary towards finer spatial and temporal resolutions.

As a final word to this article, and in agreement with the recent International Energy Agency's PVPS Task 14 conclusions [Remund et al., 2015], taking in account the fundamentals of spatial and temporal scales in the assessing the impact and developing mitigating solutions to the variability of solar resources injected of the power grid should be a prerequisite to maximize their effectiveness and minimize costs.

Acknowledgements

Many thanks to Juan Bosch of Clean Power Research for constructive comments. Part of the work presented in this paper was undertaken under the auspices of IEA-SHCP Task 46 — David Renné, Operating Agent.

References

H. Alsamamra, J. Antonio Ruiz-Arias, D. Pozo-Vazquez, and J. Tovar-Pescador. A comparative study of ordinary and residual kriging techniques for mapping global solar radiation over southern spain. *Agricultural and Forest Meteorology*, 149:1343–1357, 2009.

R. U. Antonanzas, F. J. Martinez-de-Pison, and F. Antonanzas-Torres. Solar irradiation mapping with exogenous data from support vector regression machines estimations. *Energy Conversion and Management*, 100:380–390, 2015.

E. Arias-Castro, J. Kleissl, M. Lave, J. Schweinsberg, and R Williams. A poisson model for anisotropic solar ramp rate correlations. *Solar Energy*, 101:192–202, 2013.

J. Badosa, M. Haeffelin, and H. Chepfer. Scales of spatial and temporal variation of solar irradiance on reunion tropical island. *Solar Energy*, 88: 42–56, 2013.

S. Becker et al. Features of a fully renewable US electricity system: Optimized mixes of wind and solar PV and transmission grid extensions. *Energy*, 72: 443–458, 2014.

J. Bing, P. Krishnani, O. Bartholomy, T. Hoff, and R. Perez. Solar monitoring, forecasting, and variability assessment at SMUD. In *Proceedings of the World Renewable Energy Forum*. Denver, CO, 2012.

W. Bland and M. Clayton. Spatial structure of solar radiation in Wisconsin. *Agricultural and Forest Meteorology*, 69:75–84, 1994.

J. L. Bosch and J. Kleissl. Cloud motion vectors from a network of ground sensors in a solar power plant. *Solar Energy*, 95:13–20, 2013.

J. L. Bosch, Y. Zheng, and J. Kleissl. Deriving cloud velocity from an array of solar radiation measurements. *Solar Energy*, 87:196–203, 2013.

E. Boudewijn and W. van Sark. Power output variability in randomly spaced Dutch urban rooftop solar photovoltaic systems. *IEEE*, 2013.

E. Boudewijn and W. van Sark. Spatial power fluctuation correlations in urban rooftop photovoltaic systems. In *Progress in Photovoltaics: Research and Applications*. Wiley Online Library, 2014. DOI: 10.1002/pip.2539.

P. A. Burrough and McDonnell. *Principles of Geographical Information Systems*. Oxford: Claredon Press, 1998.

W. Buytaert, R. Ce lleri, B. Bie Vre, F. Cisneros, G. Wyseure, J. Deckers, and R. Hofstede. Human impact on the hydrology of the andean paramos. *Earth-Science Review*, 79:53–72, 2006.

A. Chen, P. Chin, W. Forrest, P. McLean, and C. Grey. Solar radiation in Jamaica. *Solar Energy*, 53(5):455–460, 1994.

Z. Chuanyan, N. Zhongren, and C. Guodong. Methods for modelling of temporal and spatial distribution of air temperature at landscape scale in the southern qilian mountains, China. *Ecological Modelling*, 189:209–220, 2005.

Clean Power Research. Behind-the-meter intelligence for distributed PV grid integration. White paper, 2012. Available at http://www.cleanpower.com/wp-content/uploads/SA-FleetView-Whitepaper-v060812.pdf.

V. Dagostino and A. Zelenka. Supplementing solar radiation network data by co-kriging with satellite images. *International Journal of Climatology*, 12: 749–761, 1992.

M. David, F. Andriamasomanana, and O. Liandrat. Spatial and temporal variability of PV output in an insular grid: Case of reunion island. *Energy Procedia*, 57:1275–1282, 2014.

J. Frank, J. Freedman M. Brower, and M. Schnitzer. Development of high frequency solar data. In *Proceedings of the American Solar Energy Society Conference*, Raleigh, NC, 2011.

V. Fung, J. L. Bosch, S. Roberts, and J. Kleissl. Cloud shadow speed sensor. *Atmospheric Measurement Techniques*, 7:1693–1700, 2014. DOI: 10.5194/amt-7-1693-1700.

T. Gneiting. Nonseparable, stationary covariance functions for space-time data. *Journal of the American Statistical Association*, 97(458):590–600, 2002. Available at http://www.jstor.org/stable/3085674.

T. Gneiting, M. G. Genton, and P. Guttorp. Geostatistical space–time models, stationarity, separability and full symmetry. Technical Report 475, Department of Statistics, University of Washington, 2007. Available at http://www.stat.washington.edu/research/reports/2005/tr475.pdf.

F. Gutierrez-Corea, M. Manso-Callejo, M. Moreno-Regidor, and J. Velasco-Gomez. Spatial estimation of sub-hour global horizontal irradiance based on official observations and remote sensors. *Sensors*, 14:6758–6787, 2001.

G. Halász and Y. Malachi. Solar energy from negev desert, Israel: Assessment of power fluctuations for future PV fleet. *Energy for Sustainable Development*, 21:20–29, 2014.

T. M. Hamill and T. Nehrkorn. A short-term cloud forecast scheme using cross correlations. *Weather & Forecasting*, 8-4:401–411, 1993.

T. Hengl. A practical guide to geostatistical mapping of environmental variables. EUR 22904 EN Scientific and Technical Research series, Luxemburg: Office for Official Publications of the European Communities, pp. 143, 2007.

L. R. Hinkelmann. Differences between along-wind and cross-wind solar variability. *Proceedings of Solar Energy*, 88:192–203, 2013.

T. E. Hoff and R. Perez. Quantifying PV power output variability. *Solar Energy*, 84:1782–1793, 2010.

T. E. Hoff and R. Perez. Modeling PV fleet output variability. *Solar Energy*, 86(8):2177–2189, 2012a.

T. E. Hoff and R. Perez. Predicting short-term variability of high-penetration PV. In *Proceedings of the World Renewable Energy Forum*, Denver, CO, 2012b.

R. Holger, M. Schroedter-Homscheidt, H. G. Beyer, F. Meier, and G. Heilscher. Wolkenindikatoren für die sammelschienenspannung von niederspannungsverteilnetztransformatoren. In *29. Symposium Photovoltaische Solarenergie*, 12. bis 14. März 2014,Kloster Banz, Bad Staffelstein, 2014a.

R. Holger, M. Schroedter-Homscheidt, F. Meier, and G. Heilscher. Application of meteorological data for state estimation of an electrical low voltage grid with a high amount of photovoltaic systems. In *14th EMS Annual Meeting & 10th European Conference on Applied Climatology (ECAC)*, Prague, 2014b.

J. Huang, A. Troccoli, and P. Coppin. An analytical comparison of four approaches to modelling the daily variability of solar irradiance using meteorological records. *Renewable Energy*, 72:195–202, 2014.

R. H. Inman, H. T. C. Pedro, and C. F. M. Coimbra. Solar forecasting methods for renewable energy integration. *Progress in Energy and Combustion Science*, 39:535–576, 2013.

T. Inoue, T. Sasaki, and T. Washio. Spatio-temporal kriging of solar radiation incorporating direction and speed of cloud movement. In *The 26th Annual Conference of the Japanese Society for Artificial Intelligence*, Yamaguchi city, 2012.

S. Jamaly, J. Bosch, and J. Kleissl. Aggregate ramp rates of distributed photovoltaic systems in san diego county. *IEEE Transactions on Sustainable Energy*, 4(2):519–526, 2012. DOI: 10.1109/TSTE.2012.2201966.

E. H. Jarvis and N. Stuart. A comparison among strategies for interpolating maximum and minimum daily air temperatures. *Journal of Applied Meteorology*, 40:1075–1084, 2001.

M. Journée and C. Bertrand. Improving the spatio-temporal distribution of surface solar radiation data by merging ground and satellite measurements. *Remote Sensing of Environment*, 114:2692–2704, 2010. DOI: 10.1016/j.rse.2010.06.010.

A. Kankiewicz, M. Sengupta, and J. Li. Cloud meteorology and utility scale variability. In *Proceedings of the American Solar Energy Society Conference*, Raleigh, NC, 2011.

T. Kato, T. Inoue, and Y. Suzuki. Estimation of total power output fluctuation of high penetration photovoltaic power generation system. In *Proceedings of the IEEE Power and Energy Society General Meeting*, Detroit, Michigan, USA, 2011.

D. Krige. A statistical approach to some basic mine valuation problems on the Witwatersrand. *Journal of the Chemical, Metallurgical and Mining Society of South Africa*, 52(6):119–139, 1951.

S. Kuszamaul, A. Ellis, J. Stein, and L. Johnson. Lanai high-density irradiance sensor network for characterizing solar resource variability of MW-scale PV system. In *35th Photovoltaic Specialists Conference*, Honolulu, HI, 2010.

M. Lave and J. Kleissl. Solar intermittency of four sites across the state of colorado. *Renewable Energy*, 35:2867–2873, 2010.

M. Lave and J. Kleissl. Cloud speed impact on solar variability scaling — application to the wavelet variability model. *Solar Energy*, 91:11–21, 2013. DOI: 10.1016/j.solener.2013.01.023.

M. Lave, J. Kleissl, and E. Arias-Castro. High-frequency fluctuations in clear-sky index. *Solar Energy*, 2011. DOI: 10.1016/j.solener.2011.06.031.

M. Lave, J. Kleissl, and J. Stein. A wavelet-based variability model (WVM) for solar PV powerplants. *IEEE Transactions on Sustainable Energy*, 99, 2013. DOI: 10.1109/TSTE.2012.2205716.

M. Lipperheide, J. L. Bosch, and J. Kleissl. Embedded nowcasting method using cloud speed persistence for a photovoltaic power plant. *Solar Energy*, 112:232–238, 2015.

V. Lonij, A. Brooks, A. Cronin, M. Leuthold, and K. Koch. Intra-hour forecasts of solar power production using measurements from a network of irradiance sensors. *Solar Energy*, 97:58–66, 2013a.

V. Lonij, A. E. Brooks, A. D. Cronin, M. Leuthold, and K. Koch. Intra-hour forecasts of solar power production using measurements from a network of irradiance sensors. *Solar Energy*, 97:58–66, 2013b.

E. Lorenz, T. Scheidsteger, J. Hurka, D. Heinemann, and C. Kurz. Regional PV power prediction for improved grid integration. *Progress in Photovoltaics*, 19(7):757–771, 2011.

S. Lovejoy. Area-perimeter relation for rain and cloud areas. *Science, New Series*, 216(4542):185–187, 1982.

J. Marcos, L. Morroyo, E. Lorenzo, and M. Garcia. Smoothing of PV power fluctuations by geographical dispersion. *Progress in Photovoltaics Research Applications*, 20:226–237, 2012.

B. M. Mazumdar, M. Saquib, and A. K. Das. An empirical model for ramp analysis of utility-scale solar PV power. *Solar Energy*, 107:44–49, 2013.

D. W. McKenney, S. Pelland, Y. Poissant, R. Morris, M. Hutchinson, P. Papadopol, K. Lawrence, and K. Campbell. Spatial insolation models for photovoltaic energy in Canada. *Solar Energy*, 82(11):1049–1061, 2008.

G. G. Merino, D. Jones, D. E. Stooksbury, and K. G. Hubbard. Determination of semivariogram models to krige hourly and daily solar irradiance in western Nebraska. *Journal of Applied Meteorology and Climatology*, 40(6): 1085–1094, 2001.

A. Mills and R. Wiser. Implications of wide-area geographic diversity for short-term variability of solar power. Lawrence Berkeley National Laboratory Technical Report LBNL-3884E, 2010.

A. Moreno, M. Gilabert, and B. Martinez. Mapping daily global solar irradiation over spain: A comparative study of selected approaches. *Solar Energy*, 85(9):2072–2084, 2011.

A. Murata, H. Yamaguchi, and K. Otani. A method of estimating the output fluctuation of many photovoltaic power generation systems dispersed in a wide area. *Electrical Engineering in Japan*, 166(4):9–19, 2009.

NASA SSE. Surface meteorology and solar energy, 2012. Available at http://eosweb.larc.nasa.gov/sse/.

D. Nguyen, M. Velay, J. Schoene, V. Zhegov, B. Kurtz, K. Murray, B. Torre, and J. Kleissl. High PV penetration impacts on five local distribution networks using high resolution solar resource assessment with sky imager and quasi-steady state distribution system simulations. *Solar Energy*, 132: 221–235, 2016.

B. L. Norris and T. E. Hoff. Determining storage reserves for regulating solar variability. In *Electrical Energy Storage Applications and Technologies Biennial International Conference*, 2011.

M. Ole-Morten, G. Yordanov, and I. Ranaweera. Short-term intermittency of solar irradiance in southern Norway. In *Proceedings of the 29th European Photovoltaic Solar Energy Conference and Exhibition*, pages 2635–2638, WIP Renewable Energies, 2014.

M. J. R. Perez. Geographic dispersion and curtailment of vls-pv electricity. IEA PVPS Task 8 report, Chapter 4 Future Technical Options for the Entire Energy System, Forthcoming, 2015.

M. J. R. Perez and V. Fthenakis. Quantifying long time scale solar resource variability. In *Proceedings of the World Renewable Energy Forum*, Denver, CO, 2012.

M. J. R. Perez and V. Fthenakis. On the spatial decorrelation of stochastic solar resource variability at long timescales. *Solar Energy*, 117:46–58, 2015.

R. Perez and T. Hoff. Solar resource variability. In J. Kleissl, editor, *Solar Resource Assessment and Forecasting*, Elsevier, 2013.

R. Perez, P. Ineichen, R. Seals, and A. Zelenka. Making full use of the clearness index for parameterizing hourly insolation conditions. *Solar Energy*, 45: 111–114, 1990.

R. Perez, T. Hoff, and S. Kivalov. Spatial & temporal characteristics of solar radiation variability. In *Proceedings of the International Solar Energy (ISES) World Congress*, Kassel, Germany, 2011.

R. Perez, S. Kivalov, J. Schlemmer, C. Hemker Jr., and T. E. Hoff. Parameterization of site-specific short-term irradiance variability. *Solar Energy*, 85:1343–1353, 2011b.

R. Perez, S. Kivalov, J. Schlemmer, C. Hemker Jr., and T. E. Hoff. Short-term irradiance variability correlation as a function of distance. *Solar Energy*, 86:2170–2176, 2012.

R. Perez, T. Hoff, J. Dise, D. Chalmers, and S. Kivalov. Mitigating short-term PV output variability. In *Proceedings of the 28th European Photovoltaic Solar Energy Conference and Exhibition (EUPVSEC)*, Paris, France, 2013.

R. Perez, A. Kankiewicz, J. Schlemmer, K. Hemker Jr., and S. Kivalov. A new operational solar resource forecast service for PV fleet simulation. In *The 40th IEEE PV Specialists Conference*, 2014.

R. Perez, J. Schlemmer, K. Hemker Jr., S. Kivalov, A. Kankiewicz, and C. Gueymard. Satellite-to-irradiance modeling — a new version of the SUNY model. In *The 42nd IEEE PV Specialists Conference*, 2015.

PREPA — Puerto Rico Energy Authority, 2013. URL: www.prepa.com.

S. Rehman and S. G. Ghori. Spatial estimation of global solar radiation using geostatistics. *Renewable Energy*, 21:583–605, 2000.

J. Remund, C. Calhau, D. Marcel, and L. Perret. Spatio-temporal variability of PV production. In *Proceedings of the European Photovoltaic Solar Energy Conference and Exhibition (EUPVSEC)*, Hamburg, Germany, 2015.

I. H. Rowlands, B. P. Kemery, and I. Beausoleil-Morrison. Managing solar-PV variability with geographical dispersion: An Ontario (Canada) case-study. *Renewable Energy*, 68:171–180, 2014.

P. D. Sampson and P. Guttorp. Nonparametric estimation of nonstationary spatial covariance structure. *Journal of the American Statistical Association*, 87(417):108–119, 1992.

M. Schlather. Some covariance models based on normal scale mixtures. *Bernoulli*, 16(3):780–797, 2010. DOI: 10.3150/09-BEJ226.

M. Sengupta. Measurement and modeling of solar and PV output variability. In *Proceedings of the American Solar Energy Society Conference*, Raleigh, NC, 2011.

K. Shinozaki, N. Yamakawa, T. Sasaki, and T. Inoue. Areal solar irradiance estimated by sparsely distributed observations of solar irradiance. *IEEE Transactions on Power Systems*, 2014. TPWRS-00139-2014.R1.

A. Skartveit and J. A. Olseth. The probability density of autocorrelation of short-term global and beam irradiance. *Solar Energy*, 46(9):477–488, 1992.

J. Stein, A. Ellis, C. Hansen, and V. Chadliev. Simulation of 1-minute power output from utility-scale photovoltaic generation systems. In *Proceedings of the American Solar Energy Society Conference*. Raleigh, NC, 2011.

G. M. Stokes and S. E. Schwartz. The atmospheric radiation measurement (arm) program: Programmatic background and design of the cloud and radiation test bed. *Bulletin of American Meteorological Society*, 75:1201–1221, 1994.

G. Q. Tabios and J. D. Salas. A comparative analysis of techniques for spatial interpolation of precipitation. *Water Resource Research*, 21:365–380, 1985.

T. Tomson. Fast dynamic processes of solar radiation. *Solar Energy*, 84(2): 318–323, 2009.

B. Urquhart, B. Kurtz, E. Dahlin, M. Ghonima, J. E. Shields, and J. Kleissl. Development of a sky imaging system for short-term solar power forecasting. *Atmospheric Measurement Techniques Discussion*, 7:4859–4907, 2014. DOI: 10.5194/amtd-7-4859-2014.

F. Vignola. Variability of solar radiation over short time intervals. In *Proceedings of the American Solar Energy Society Conference*. Washington, D.C, 2001.

F. Vignola, A. C. McMahan, and C. N. Grover. Bankable solar-radiation datasets. In *Solar Energy Forecasting and Resources Assessment*, Elsevier Press, 2013.

J. M. Vindel and J. Polo. Intermittency and variability of daily solar irradiation. *Atmospheric Research*, 143:313–327, 2014.

E. Wiemken, H. G. Beyer, W. Heydenreich, and K. Kiefer. Power characteristics of PV ensembles: Experience from the combined power productivity of 100 grid-connected systems distributed over Germany. *Solar Energy*, 70: 513–519, 2001.

A. Woyte, R. Belmans, and J. Nijs. Fluctuations in instantaneous clearness index: Analysis and statistics. *Solar Energy*, 81(2):195–206, 2007.

D. Yang, C. Gu, Z. Dong, P. Jirutitijaroen, N. Chen, and W. M. Walsh. Solar irradiance forecasting using spatial–temporal covariance structures and time–forward kriging. *Renewable Energy*, 60:235–245, 2013.

D. Yang, Z. Dong, T. Reindl, P. Jirutitijaroen, and W. M. Walsh. Solar irradiance forecasting using spatio–temporal empirical kriging and vector autoregressive models with parameter shrinkage. *Solar Energy*, 103:550–562, 2014a.

H. Yang, B. Kurtz, A. Nguyen, B. Urquhart, C. W. Chow, M. Ghonima, and J. Kleissl. Solar irradiance forecasting using a ground-based sky imager developed at UC San Diego. *Solar Energy*, 103:502–524, 2014b.

G. Yordanov, O. Mitdgard, and L. Norum. Overirradiance (cloud enhancement) events at high latitudes. *IEEE Journal of Photovoltaics*, 3(1):271–278, 2013.

A. Zagouras, H. T. C. Pedro, and C. F. M. Coimbra. On the role of lagged exogenous variables and spatiotemporal correlations in improving the accuracy of solar forecasting methods. *Renewable Energy*, 78:203–218, 2015.